

Effect of carbon on the room temperature compressive behaviour of Ti-44.5Al-8Nb-0.8Mo- x C alloys prepared by vacuum induction melting

M. Štamborská*, J. Lapin, O. Bajana

*Institute of Materials & Machine Mechanics, Slovak Academy of Sciences,
Dúbravská cesta 9, 845 13 Bratislava, Slovak Republic*

Received 18 September 2018, received in revised form 9 November 2018, accepted 9 November 2018

Abstract

The effect of carbon content x ranging from 1.4 to 3.6 at.% on the room temperature compressive behaviour of Ti-44.5Al-8Nb-0.8Mo- x C (at.%) alloys prepared by vacuum induction melting has been studied. The microstructural analysis by SEM shows that the increase of the carbon content increases the volume fraction of the reinforcing carbide particles and leads to a change of the matrix microstructure from $\alpha_2(\text{Ti}_3\text{Al}) + \gamma(\text{TiAl}) + \beta/\text{B2}$ to γ type. The carbon content affects the morphology and size of the primary plate-like, regular and irregular shaped Ti_2AlC particles. The finite element analysis (FEA) of local equivalent strains and quantitative metallography analysis indicate that the mean size of fragmented carbide particles decreases with increasing local equivalent strain in the compression specimens. The differences in work hardening behaviour of the compression specimens with various content of carbon are related to the initial non-uniform deformation, cracking of primary carbide particles, crack propagation and release of some grains from the free surface during compression testing.

Key words: TiAl, composites, mechanical properties, microstructure, finite element analysis

1. Introduction

Intermetallic TiAl-based alloys are attractive materials characterised by a low density (about 4 g cm^{-3}), high-temperature strength, excellent creep strength, good resistance to oxidation and hot gas corrosion [1, 2]. These alloys have been introduced successfully as innovative lightweight structural high-temperature materials into aero and automotive combustion engines, e.g. as turbine blades or turbocharger wheels [3, 4]. However, low room-temperature ductility and insufficient strength at high temperatures (above 800°C) limit the extensive application of TiAl-based alloys [2]. The high-temperature strength of TiAl-based alloys can be improved by the addition of interstitial elements, such as carbon [5, 6]. While low additions of carbon lead to the formation of fine P- Ti_3AlC and H- Ti_2AlC precipitates [7, 8], the increase of carbon content above 1 at.% results in the formation of pri-

mary Ti_2AlC particles directly from the melt during solidification [9–11]. Recent studies have shown that TiAl-based alloys reinforced with homogeneously distributed coarse carbide particles can be prepared by melting and casting techniques [10–17]. In spite of the previous studies, only very limited information is available about the room temperature compressive behaviour of high carbon containing TiAl-based alloys prepared by melting and casting. Several authors [18–20] have reported that an increase of volume fraction of Ti_2AlC particles increases room temperature compressive strength of the alloys prepared by arc melting or combustion synthesis. On the other hand, Lapin et al. [10] have reported a decrease of room temperature compressive strength with increasing volume fraction of Ti_2AlC particles in the alloys prepared by centrifugal casting. Since the casting represents widely applied technology which might facilitate potential applications of novel systems [11, 21, 22], it is of large inter-

*Corresponding author: tel.: +421 2 3240 1058; e-mail address: michaela.stamborska@savba.sk

Table 1. The measured chemical composition of the compression specimens

Compression specimens	Element (at.%)				
	Ti	Al	Nb	Mo	C
C1.4	45.5 ± 0.1	44.2 ± 0.4	8.1 ± 0.1	0.8 ± 0.2	1.4 ± 0.1
C2.5	44.5 ± 0.1	44.2 ± 0.3	8.1 ± 0.1	0.7 ± 0.3	2.5 ± 0.1
C3.6	43.2 ± 0.5	44.6 ± 0.5	7.9 ± 0.1	0.7 ± 0.2	3.6 ± 0.2

est to investigate the room temperature compressive behaviour of TiAl-based alloys reinforced with the various volume fractions of coarse primary Ti_2AlC particles prepared by melting and casting.

The aim of this article is to study the effect of carbon content x ranging from 1.4 to 3.6 at.% on the room temperature compressive behaviour of Ti-44.5Al-8Nb-0.8Mo- x C (at.%) alloys prepared by vacuum induction melting. Experimental measurements and finite element analysis (FEA) are carried out to characterise the compressive behaviour of these alloys. Numerically calculated local strains within the specimens after compression tests are related to the size of fragmented carbide particles.

2. Experimental procedures

The studied alloys with the carbon content ranging from 1.4 to 3.6 at.% were prepared by vacuum induction melting in the graphite crucibles [23] which was followed by a centrifugal casting (CC) into a cold graphite mould under argon atmosphere [10, 11]. The as-cast conical samples with a diameter ranging from 15 to 17 mm and length of 150 mm were subjected to hot isostatic pressing (HIP) at a temperature of 1250 °C and applied pressure of 200 MPa for 4 h in argon to remove casting porosity. The hot isostatic pressing was followed by annealing at a temperature of 900 °C for 25 h in air.

Cylindrical specimens with a diameter of 8 mm and length of 12 mm were used for compression tests. The surface of the compression specimens was polished to a roughness better than 0.3 μm using a diamond paste. The uniaxial room temperature compression tests were carried out at an initial strain rate of $1 \times 10^{-4} \text{ s}^{-1}$ up to a true strain of 15% using a universal testing machine. The compressive deformation was measured by a contactless laser extensometer. Vickers microhardness measurements were performed at an applied load of 0.25 N and loading time of 10 s at room temperature on polished and slightly etched specimens before and after compression testing.

Metallographic preparation of the samples consisted of standard grinding on abrasive papers and polishing on diamond pastes with various grain sizes up to 0.25 μm . The samples for Vickers microhard-

ness measurements were slightly etched in a reagent of 150 ml H_2O , 25 ml HNO_3 and 10 ml HF. The microstructural evaluation was carried out by scanning electron microscopy (SEM) and SEM in backscattered electron (BSE) mode. Energy dispersive spectroscopy (EDS) calibrated using standards was applied for measurements of the chemical composition of the alloys. The average content of carbon was measured by LECO CS844 elemental analyser based on the combustion method. The quantitative metallographic analysis was performed on digitalised BSE micrographs using computerised image analyser. The achieved microstructural data were treated statistically.

The numerical simulation was realised with a software Ansys Workbench. A geometry model of compression specimen was built as a 3D cylinder with a diameter of 8 mm and length of 12 mm. Material model was built up using the achieved experimental data from the compression tests at room temperature. For 3D analysis, deformable hexahedron elements with a size of 0.6 mm were used to mesh the cylindrical compression specimen.

3. Results and discussion

3.1. The microstructure of compression specimens before testing

The chemical compositions of the studied compression specimens with the carbon content ranging from 1.4 to 3.6 at.% are summarised in Table 1 [10]. Figure 1 shows the typical microstructures of the compression specimens prepared from centrifugally cast C1.4, C2.5 and C3.6 samples after HIP and annealing at 900 °C for 25 h. The microstructure of the specimens consists of intermetallic $\gamma(\text{TiAl})$ -based matrix and coarse primary $\text{H-Ti}_2\text{AlC}$ particles [10]. The carbide particles, which are formed during solidification in the melt, are relatively homogeneously distributed in the intermetallic matrix, as shown in Figs. 1a–c. Three morphologically different types of the primary $\text{H-Ti}_2\text{AlC}$ particles can be identified in the matrix: regular shaped (R), plate-like (P) and irregular shaped (I) ones. While the matrix of the specimens C1.4 (Fig. 1a) and C2.5 (Fig. 1b) remains still pseudo-duplex [24] composed of the lamellar $\alpha_2 + \gamma$ regions

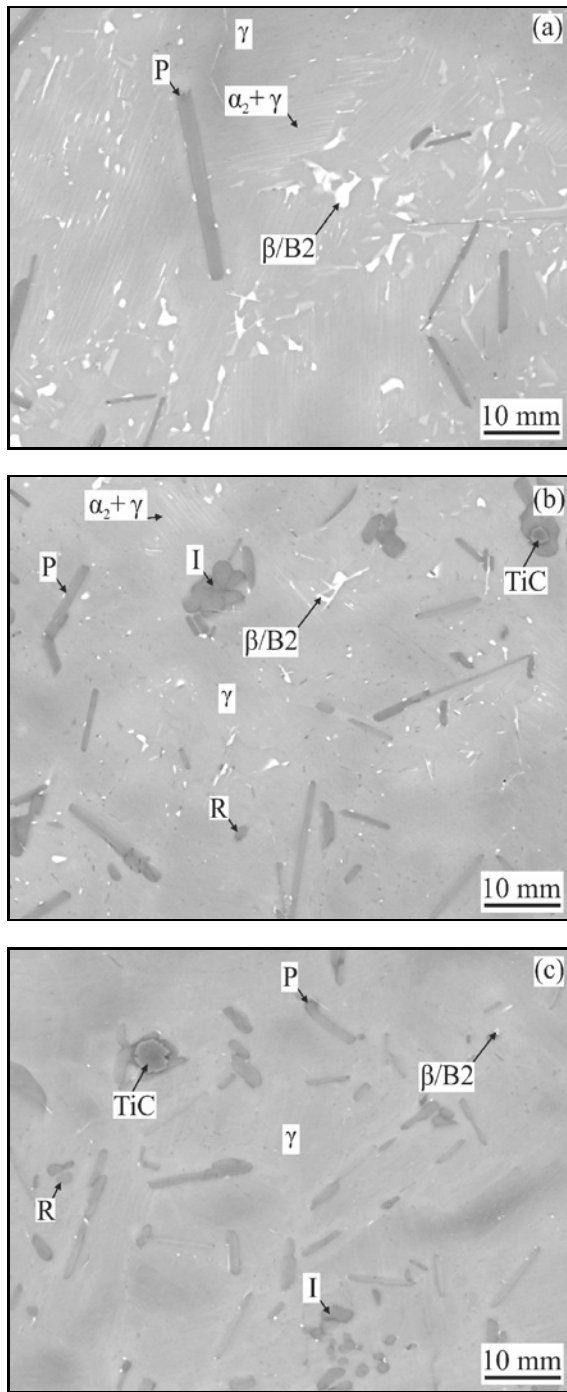


Fig. 1. BSE micrographs showing the typical microstructure of the compression specimens: (a) C1.4; (b) C2.5; (c) C3.6. P – plate-like, R – regular shaped and I – irregular shaped primary Ti_2AlC particles.

with some β/B_2 particles and single γ phase regions, the matrix of the specimen C3.6 (Fig. 1c) changes to near γ due to full dissolution of the α_2 phase. In all studied alloys, the partial or full dissolution of the α_2 phase leads to the precipitation of fine secondary carbide particles [13, 25].

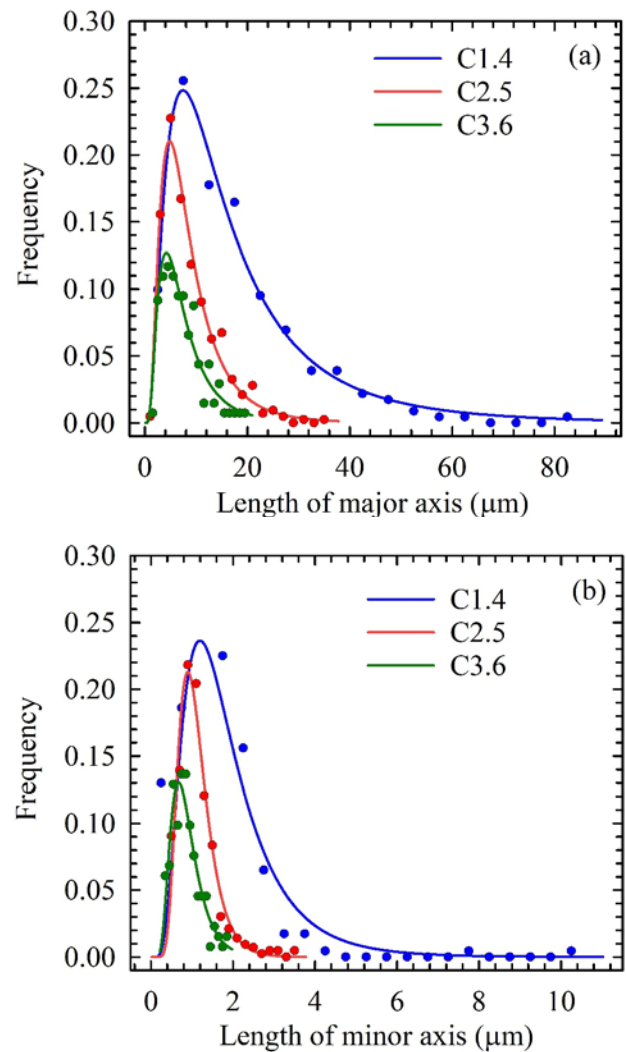


Fig. 2. Log-normal distribution curves of the size of primary plate-like carbide particles before compression testing: (a) length of the major axis; (b) length of the minor axis.

Figure 2 shows the typical examples of distribution curves of the measured size of the primary carbide particles before compression testing (BC). Both the length of the major axis (Fig. 2a) and length of the minor axis (Fig. 2b) can be fitted by a log-normal distribution function. Table 2 summarises mean length of the major axis, mean length of the minor axis, average shape factor defined elsewhere [26] and volume fraction of the regular, plate-like and irregular shaped primary carbide particles in the specimens before compression testing. The increase in the carbon content from 1.4 to 3.6 at.% leads to an increase in the volume fraction of the primary carbide particles from 6.0 to 14.9 vol.%. While the specimen C1.4 contains only plate-like Ti_2AlC particles, the specimens C2.5 and C3.6 contain plate-like, irregular and regular shaped ones. In addition, the specimens C1.4 and C2.5 con-

Table 2. Length of the major axis, length of the minor axis, shape factor and volume fraction of primary plate-like (P), regular shaped (R) and irregular shaped (I) carbide particles in the middle regions (M) and vicinity of the contact areas (U) of the specimens before (BC) and after compression (AC) tests

Specimens	Shape of state carbides	Parameter							
		Length of the major axis (μm)		Length of the minor axis (μm)		Shape factor		Volume fraction (vol.%)	
		Region	U	M	U	M	U		M
C1.4	P	BC	7.5 ± 0.2		1.2 ± 0.1		0.24 ± 0.01		6.0 ± 0.3
		AC	7.5 ± 0.1	3.1 ± 0.1	1.3 ± 0.1	1.0 ± 0.1	0.21 ± 0.01	0.37 ± 0.03	
		β (vol.%)	1.3 ± 0.1						
	R	BC	2.2 ± 0.1		1.1 ± 0.1		0.71 ± 0.01		1.2 ± 0.4
AC		2.3 ± 0.1	2.0 ± 0.1	1.2 ± 0.1	1.1 ± 0.1	0.70 ± 0.01	0.81 ± 0.01		
C2.5	P	BC	4.8 ± 0.2		0.9 ± 0.1		0.32 ± 0.02		4.6 ± 0.3
		AC	4.8 ± 0.1	3.4 ± 0.1	0.9 ± 0.1	0.9 ± 0.1	0.34 ± 0.01	0.43 ± 0.01	
	I	BC	5.4 ± 0.1		2.7 ± 0.1		0.48 ± 0.02		4.6 ± 0.3
		AC	5.5 ± 0.1	4.4 ± 0.2	2.7 ± 0.1	1.6 ± 0.1	0.46 ± 0.02	0.53 ± 0.02	
		TiC (vol.%)	0.2 ± 0.1						
		β (vol.%)	0.3 ± 0.1						
C3.6	R	BC	2.6 ± 0.1		1.5 ± 0.1		0.75 ± 0.01		3.1 ± 0.3
		AC	2.5 ± 0.2	2.2 ± 0.2	1.4 ± 0.1	1.1 ± 0.1	0.76 ± 0.01	0.71 ± 0.01	
	P	BC	4.2 ± 0.3		0.8 ± 0.1		0.33 ± 0.01		4.1 ± 0.2
		AC	3.7 ± 0.1	2.4 ± 0.1	0.9 ± 0.1	0.7 ± 0.1	0.39 ± 0.01	0.37 ± 0.02	
	I	BC	7.2 ± 0.5		3.8 ± 0.3		0.43 ± 0.02		7.7 ± 0.4
		AC	7.0 ± 0.4	3.8 ± 0.5	3.4 ± 0.2	1.0 ± 0.1	0.46 ± 0.01	0.55 ± 0.03	
	TiC (vol.%)	0.6 ± 0.1							

tain low volume fraction of β /B2 phase. A low volume fraction of TiC particles is identified in the specimens C2.5 and C3.6.

3.2. Compressive behaviour

3.2.1. Finite element analysis

The compression true stress-true strain curves were calculated from the measured engineering compression stress-strain data using the procedure described elsewhere [27]. Figure 3 shows the typical true stress-true strain compression curves and numerical calculations using FEA software ANSYS. It is clear from this figure that the numerical calculations are in a

very good agreement with the experimentally measured true stress-true strain curves. Figure 4 shows longitudinal sections of the compression specimens C1.4 and C3.6 and corresponding 3D numerical calculations of equivalent plastic strains. The slightly barrelled shapes of the specimens tested to a true strain of 15% (Figs. 4a, c) correspond quite well to the calculated ones (Figs. 4b, d). The FEA indicates the inhomogeneous distribution of the local calculated strains. The highest equivalent strains of 19 and 21% calculated for the compression specimens C1.4 and C3.6, respectively, are achieved in the middle regions marked by the red rectangles (M) in Figs. 4a, c. The lowest equivalent strains ranging from 4 to 10% (Figs. 4b, d) are achieved in the vicinity of the contact areas of

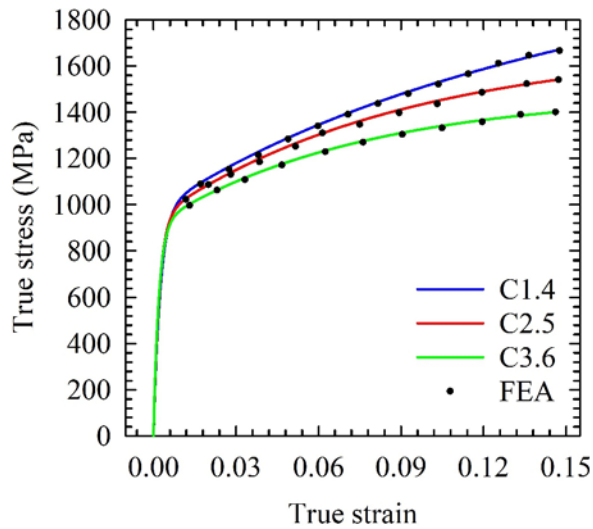


Fig. 3. Dependence of compressive true stress on true strain.

the specimens with the pressure plates of the testing machine marked by the blue rectangles (U).

3.2.2. Work hardening

Table 3 summarises the average 0.2% offset compressive yield strength (YS) and Vickers microhardness HV_m of the matrix for the specimens C1.4, C2.5 and C3.6. The increase of the carbon content leads to a decrease of both the compressive yield strength and Vickers microhardness of the matrix in the BC specimens. The increase of the Vickers microhardness in the specimens C1.4, C2.5 and C3.6 after compression testing (AC) in both the regions M and U (Table 3) and compression curves (Fig. 3) indicate a clear work-hardening during compressive deformation. Figure 5 shows the dependence of the calculated work hardening rate (WHR) on true strain and true stress. The work hardening rate is calculated as $\Theta = d\sigma_t/d\varepsilon_t$, where σ_t is the true stress and ε_t is the true strain. Two different regions can be well identified on the WHR curves, as illustrated in Fig. 5. The region I is characterised by a fast decrease of the WHR with the true strain up to 1.2, 1.3 and 1.5% (Fig. 5a) or true stress up to 1000, 1040 and 1080 MPa (Fig. 5b) for the specimens C1.4, C2.5 and C3.6, respectively. Appel et

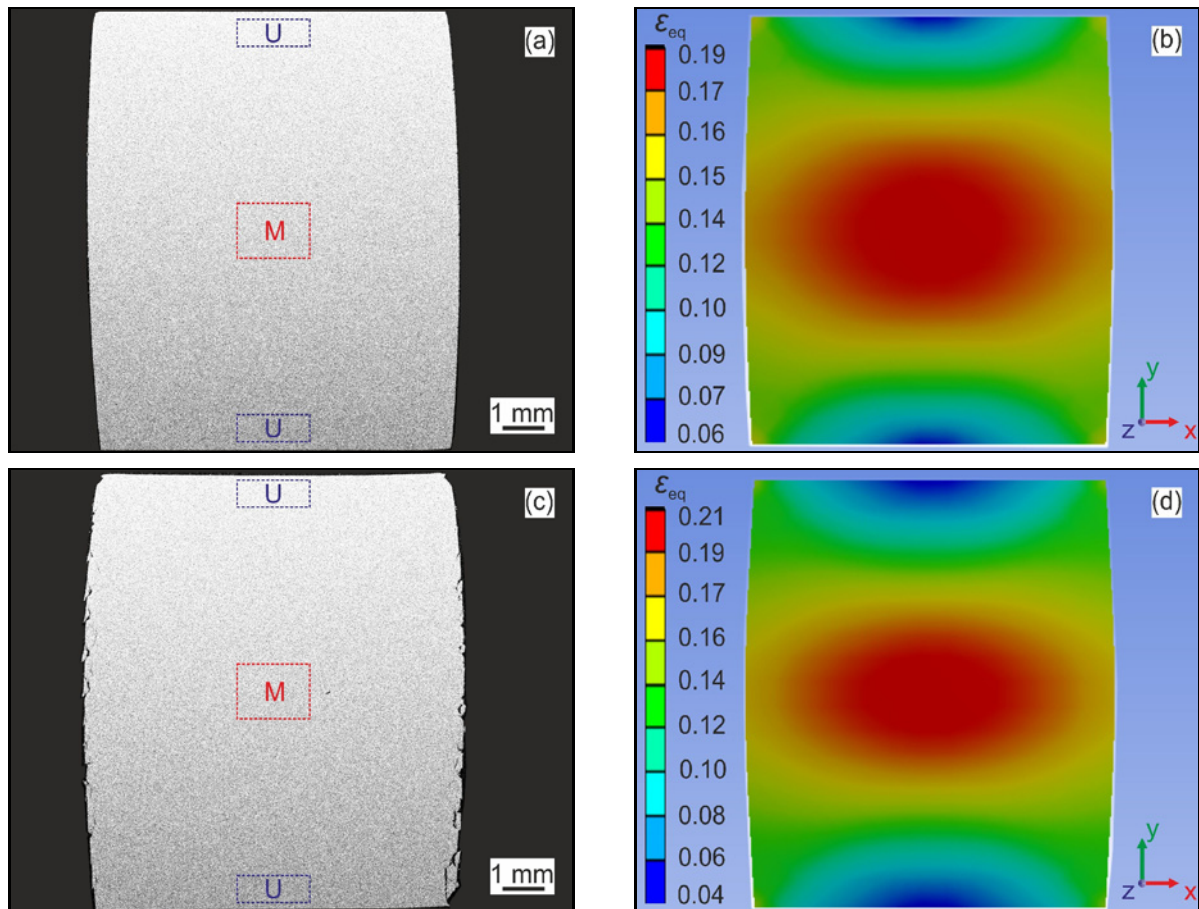


Fig. 4. Longitudinal sections of the compression specimens tested to a true strain of 15% and corresponding 3D numerical modelling of equivalent plastic strains: (a) SEM macrostructure and (b) FEA of the compression specimen C1.4; (c) SEM macrostructure and (d) FEA of the compression specimen C3.6.

Table 3. Room-temperature 0.2 % offset compressive yield strength YS and Vickers microhardness HV_m

Compression specimens	YS (MPa)	HV _m		
		BC	AC	
			U	M
C1.4	910 ± 7	438 ± 9	465 ± 8	514 ± 8
C2.5	900 ± 8	377 ± 4	426 ± 8	507 ± 4
C3.6	888 ± 8	323 ± 4	366 ± 6	415 ± 7

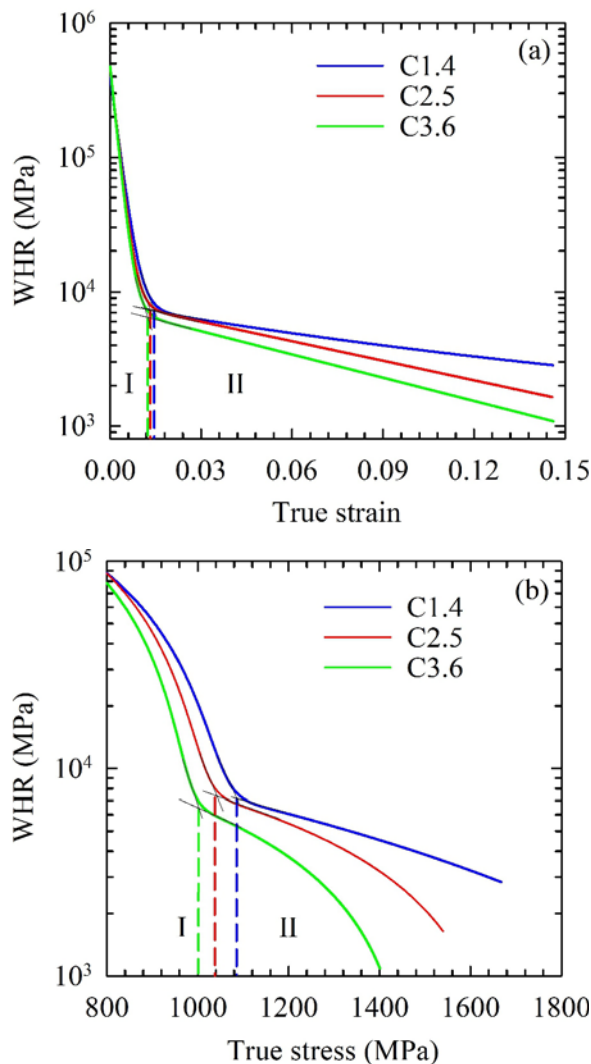


Fig. 5. (a) Dependence of work hardening rate on true strain. (b) Dependence of work hardening rate on true stress.

al. [28] have reported that a fast decrease of WHR with increasing compressive strain up to 2 % in TiAl-based alloys is connected with a non-uniform deformation starting in favourably oriented grains which leads to a reduction of constraint stresses by localised flow but it is not conventional work hardening con-

trolled by dislocation interactions. While the carbon content has a small effect on the work hardening behaviour in the region I, the evolution of the WHR with the true strain or true stress significantly differs for the specimens C1.4, C2.5 and C3.6 in the region II, as shown in Fig. 5. The increase of the carbon content in the specimens C1.4, C2.5 and C3.6 leads to a faster decrease of the WHR with increasing true strain or true stress in the region II. The high WHR measured in the region II for the specimen C1.4 can be attributed to an increase of dislocation density, very short mean free path of mobile dislocations and mechanical twinning [28–31]. The faster decrease of the WHR in the region II for the specimens C2.5 and C3.6 compared to that of the specimen C1.4 indicates an intensive softening connected with microstructure degradation during compression testing.

3.3. The microstructure of compression specimens after testing

Figure 6 shows microstructure on longitudinal sections of the compression specimens C1.4 and C3.6 deformed to a true strain of 15 %. While the matrix shows no evidence of cracking, the compressive deformation in the regions U corresponding to a local strain of about 6 % is connected with early stages of cracking of some plate-like and irregular shaped carbide particles and delamination at the carbide particle/matrix interfaces, as shown in Figs. 6a, c. The local strains up to 19 % in the region M for the specimen C1.4 lead to an intensive fragmentation of the plate-like carbide particles, as seen in Fig. 6b. The local strains up to 21 % in the region M for the specimen C3.6 lead to an intensive fragmentation of the irregular shaped and some plate-like carbide particles, as shown in Fig. 6d. In spite of relatively large local deformation, the initiation and propagation of cracks is constrained to take place within the carbide particles in the region M. However, Fig. 4c indicates that the compressive deformation in the vicinity of the free surface is connected with the initiation and propagation of numerous large cracks which can lead even to the release of some grains from the specimen surface. Figure 6e shows that such cracks propagate within the

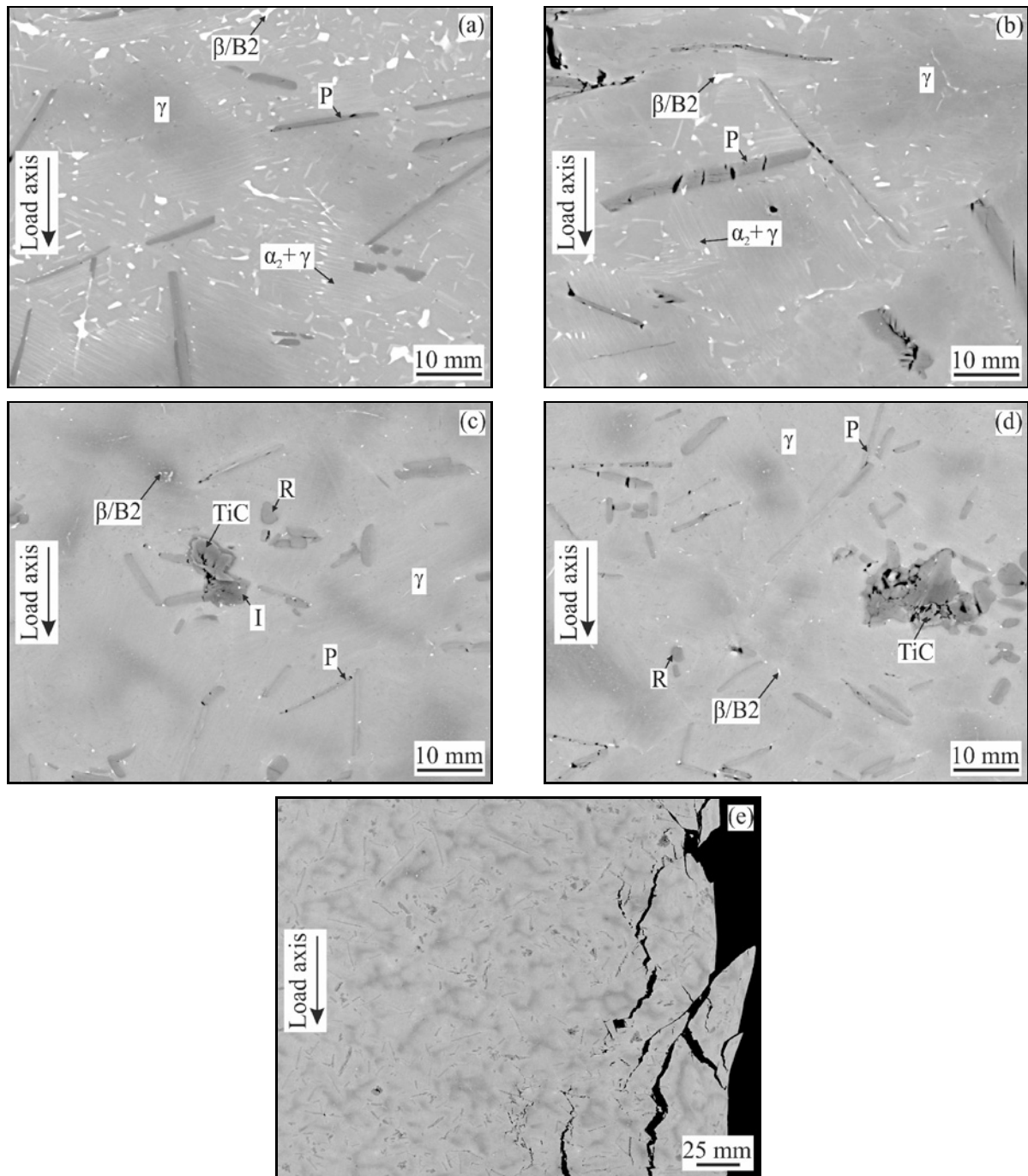


Fig. 6. BSE micrographs showing microstructure on longitudinal sections of compression specimens: (a) Crack initiation within plate-like particles in the region U of the compression specimen C1.4, local strain of 6 %; (b) Fragmentation of plate-like (P) particles in the region M of the compression specimen C1.4, local strain of 19 %; (c) Crack initiation within coarse irregular shaped particles in the region U of the compression specimen C3.6, local strain of 4 %; (d) Fragmentation of irregular (I) and plate-like (P) shaped particles in the region M of the compression specimen C3.6, local strain of 21 %; (e) Crack propagation within the matrix and carbide particles in the vicinity of free surface of compression specimen C3.6, local strain of 14 %.

matrix, carbide particles and along the γ grain boundaries. Table 2 summarises the results of statistical evaluation of mean length of major axis, mean length of minor axis and average shape factor of the fragmented plate-like, regular and irregular shaped carbide parti-

cles after the compression (AC) in the regions M and U. It is clear from this table that the fragmentation leads to a significantly smaller size of the primary carbide particles and is more intensive in the region M compared to that in the region U.

4. Conclusions

The effect of carbon on the room temperature compressive behaviour of Ti-44.5Al-8Nb-0.8Mo-*x*C (at.%) alloys prepared by vacuum induction melting has been characterised. The achieved results can be summarised as follows:

1. The increase of the carbon content from 1.4 to 3.6 at.% leads to an increase in volume fraction and morphological changes of the primary Ti₂AlC particles in the studied alloys. While the matrix of the compression specimen C1.4 is reinforced with plate-like carbide particles, the matrices of the specimens C2.5 and C3.6 are reinforced with plate-like, regular and irregular shaped primary carbides. The increase of the carbon content leads to a change of the matrix microstructure from $\alpha_2 + \gamma + \beta/B2$ to γ type in the specimens C1.4 and C3.6, respectively.

2. The local equivalent strains in the compression specimens are numerically calculated using finite element analysis software ANSYS and related to the size of fragmented primary carbide particles. The mean size of fragmented carbide particles decreases with increasing local equivalent strain in the compression specimens.

3. Two regions characterise the evolution of the work hardening rate with the true strain and true stress. The differences in work hardening behaviour of the compression specimens C1.4, C2.5 and C3.6 can be related to the initial non-uniform deformation, cracking of primary carbide particles, crack propagation and release of some grains from the free surface of the specimens.

Acknowledgements

This work was financially supported by the Slovak Research and Development Agency under the contract APVV-15-0660 and Research and Development Operational Program funded by the European Regional Development Fund under the contract ITMS 26220220146.

References

- [1] Appel, F., Paul, J. D. H., Oehring, M.: Gamma Titanium Aluminide Alloys: Science and Technology. Weinheim, ILEY-VCH Verlag & Co. KGaA 2011. [doi:10.1002/9783527636204](https://doi.org/10.1002/9783527636204)
- [2] Kim, Y. W., Kim, S. L.: JOM, 70, 2018, p. 553. [doi:10.1007/s11837-018-2747-x](https://doi.org/10.1007/s11837-018-2747-x)
- [3] Bewlay, B. P., Nag, S., Suzuki, A., Weimer, M. J.: Mater. High Temp., 33, 2016, p. 549. [doi:10.1080/09603409.2016.1183068](https://doi.org/10.1080/09603409.2016.1183068)
- [4] Clemens, H., Mayer, S.: Mater. High Temp., 33, 2016, p. 560. [doi:10.1080/09603409.2016.1163792](https://doi.org/10.1080/09603409.2016.1163792)
- [5] Tian, W. H., Nemoto, M.: Intermetallics, 5, 1997, p. 237. [doi:10.1016/S0966-9795\(96\)00086-6](https://doi.org/10.1016/S0966-9795(96)00086-6)
- [6] Appel, F., Oehring, M., Wagner, R.: Intermetallics, 8, 2000, p. 1283. [doi:10.1016/S0966-9795\(00\)00036-4](https://doi.org/10.1016/S0966-9795(00)00036-4)
- [7] Gabrisch, H., Stark, A., Schimansky, F. P., Wang, L., Schell, N., Lorenz, U., Pyczak, F.: Intermetallics, 33, 2013, p. 44. [doi:10.1016/j.intermet.2012.09.023](https://doi.org/10.1016/j.intermet.2012.09.023)
- [8] Wang, L., Oehring, M., Lorenz, U., Stark, A., Pyczak, F.: Intermetallics, 100, 2018, p. 70. [doi:10.1016/j.intermet.2018.06.006](https://doi.org/10.1016/j.intermet.2018.06.006)
- [9] Schwaighofer, E., Rashkova, B., Clemens, H., Stark, A., Mayer, S.: Intermetallics, 46, 2014, p. 173. [doi:10.1016/j.intermet.2013.11.011](https://doi.org/10.1016/j.intermet.2013.11.011)
- [10] Lapin, J., Klimová, A., Gabalcová, Z., Pelachová, T., Bajana, O., Štamborská, M.: Mater. Des., 133, 2017, p. 404. [doi:10.1016/j.matdes.2017.08.012](https://doi.org/10.1016/j.matdes.2017.08.012)
- [11] Lapin, J., Kamyshnykova, K.: Intermetallics, 98, 2018, p. 34. [doi:10.1016/j.intermet.2018.04.012](https://doi.org/10.1016/j.intermet.2018.04.012)
- [12] Song, X., Cui, H., Han, Y., Hou, N., Wei, N., Ding, L., Song, Q.: Mater. Sci. Eng. A, 684, 2017, p. 406. [doi:10.1016/j.msea.2016.12.069](https://doi.org/10.1016/j.msea.2016.12.069)
- [13] Lapin, J., Štamborská, M., Pelachová, T., Bajana, O.: Mater. Sci. Eng. A, 721, 2018, p. 1. [doi:10.1016/j.msea.2018.02.077](https://doi.org/10.1016/j.msea.2018.02.077)
- [14] Klimová, A., Lapin, J., Pelachová, T.: IOP Conf. Ser. Mater. Sci. Eng., 179, 2017, art. no. 012038. [doi:10.1088/1757-899X/179/1/012038](https://doi.org/10.1088/1757-899X/179/1/012038)
- [15] Chen, R., Tan, Y., Fang, H., Luo, L., Ding, H., Su, Y., Guo, J., Fu, H.: Mater. Sci. Eng. A, 725, 2018, p. 171. [doi:10.1016/j.msea.2018.04.025](https://doi.org/10.1016/j.msea.2018.04.025)
- [16] Fang, H., Chen, R., Gong, X., Su, Y., Ding, H., Guo, J., Fu, H.: Adv. Eng. Mater., 4, 2018, p. 1701112. [doi:10.1002/adem.201701112](https://doi.org/10.1002/adem.201701112)
- [17] Chen, R., Fang, H., Chen, X., Su, Y., Ding, H., Guo, J., Fu, H.: Intermetallics, 81, 2017, p. 9. [doi:10.1016/j.intermet.2017.02.025](https://doi.org/10.1016/j.intermet.2017.02.025)
- [18] Song, X. J., Cui, H. Z., Hou, N., Wei, N., Han, Y., Tian, J., Song, Q.: Ceram. Int., 42, 2016, p. 13586. [doi:10.1016/j.ceramint.2016.05.152](https://doi.org/10.1016/j.ceramint.2016.05.152)
- [19] Shu, S., Qiu, F., Jin, S., Lu, J., Jiang, Q.: Mater. Des., 32, 2011, p. 5061. [doi:10.1016/j.matdes.2011.05.041](https://doi.org/10.1016/j.matdes.2011.05.041)
- [20] Fang, H., Chen, R., Yang, Y., Su, Y., Ding, H., Guo, J., Fu, H.: Mater. Des., 156, 2018, p. 300. [doi:10.1016/j.matdes.2018.06.048](https://doi.org/10.1016/j.matdes.2018.06.048)
- [21] Harding, R. A.: Kovove Mater., 45, 2007, p. 1.
- [22] Bünck, M., Stoyanov, T., Schievenbusch, J., Michels, H., Gußfeld, A.: JOM, 69, 2017, p. 2565. [doi:10.1007/s11837-017-2534-0](https://doi.org/10.1007/s11837-017-2534-0)
- [23] Kamyshnykova, K., Lapin, J.: Vacuum, 154, 2018, p. 218. [doi:10.1016/j.vacuum.2018.05.017](https://doi.org/10.1016/j.vacuum.2018.05.017)
- [24] Lapin, J., Klimová, A.: Kovove Mater., 41, 2003, p. 1.
- [25] Čegan, T., Szurman, I., Kurša, M., Holešínský, J., Vontorová, J.: Kovove Mater., 53, 2015, p. 69. [doi:10.4149/km.2015-2.69](https://doi.org/10.4149/km.2015-2.69)
- [26] Štamborská, M., Lapin, J., Bajana, O., Losertová, M.: Kovove Mater., 53, 2015, p. 399. [doi:10.4149/km.2015-6.399](https://doi.org/10.4149/km.2015-6.399)
- [27] Štamborská, M., Lapin, J.: Kovove Mater., 55, 2017, p. 369. [doi:10.4149/km.2017_6_369](https://doi.org/10.4149/km.2017_6_369)
- [28] Appel, F., Sparka, U., Wagner, R.: Intermetallics, 7, 1999, p. 325. [doi:10.1016/S0966-9795\(98\)00109-5](https://doi.org/10.1016/S0966-9795(98)00109-5)
- [29] Kauffmann, F., Bidlingmaier, T., Dehm, G., Wanner, A., Clemens, H.: Intermetallics, 8, 2000, p. 823. [doi:10.1016/S0966-9795\(00\)00025-X](https://doi.org/10.1016/S0966-9795(00)00025-X)
- [30] Paul, J. D. H., Appel, F., Wagner, R.: Acta Mater., 46, 1998, p. 1075. [doi:10.1016/S1359-6454\(97\)00332-7](https://doi.org/10.1016/S1359-6454(97)00332-7)
- [31] Viguier, B.: Mater. Sci. Eng. A, 349, 2003, p. 132. [doi:10.1016/S0921-5093\(02\)00785-2](https://doi.org/10.1016/S0921-5093(02)00785-2)